Auroral processes in satellite data

Tomas Karlsson

Space and Plasma Physics, School of Electrical Engineering
Royal Institute of Technology, Stockholm
Sweden

Overview

- Setting the scene
- Auroral processes in the upward current region
- Auroral processes in the downward current region
- Dayside and cusp aurora, theta aurora
- Temporal evolution in the auroral zone

Very useful reference:

Space Science Series of ISSI

Auroral Plasma Physics

Götz Paschmann, Stein Haaland, Rudolf Treumann

(Space Science Reviews, vol 103, 1-4, 2002)

Auroral ovals

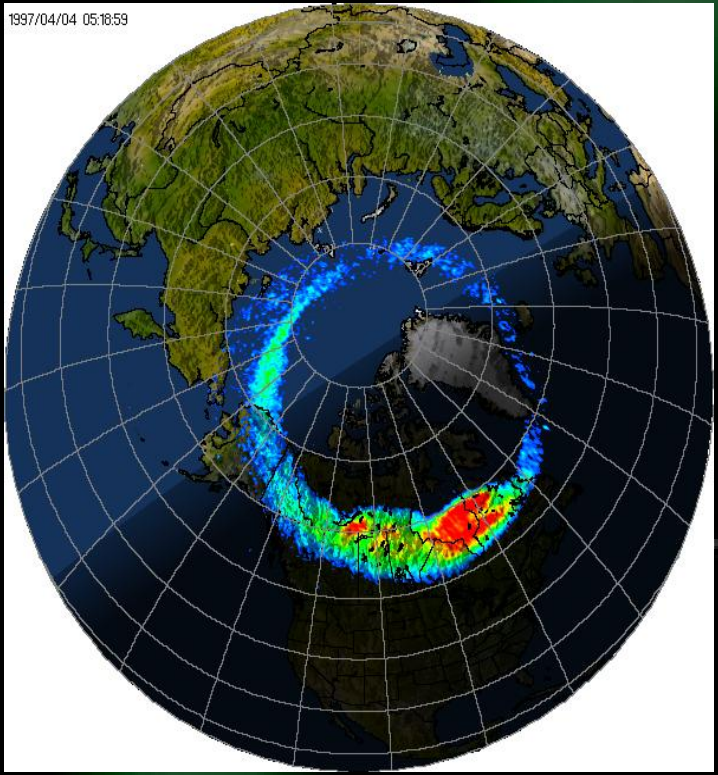

Polar

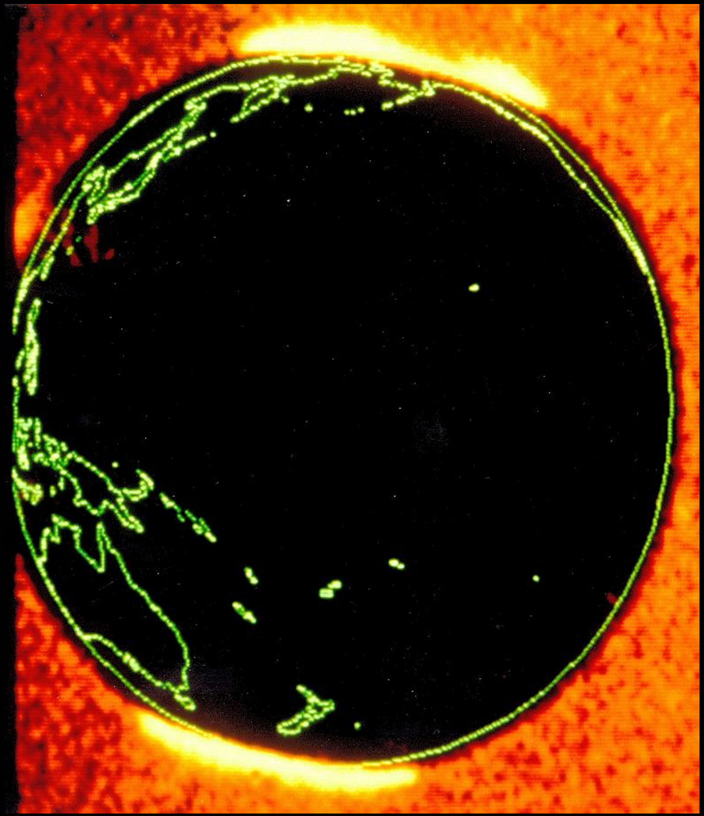

Dynamics Explorer

The auroral oval is the projection of the plasmasheet onto the atmosphere

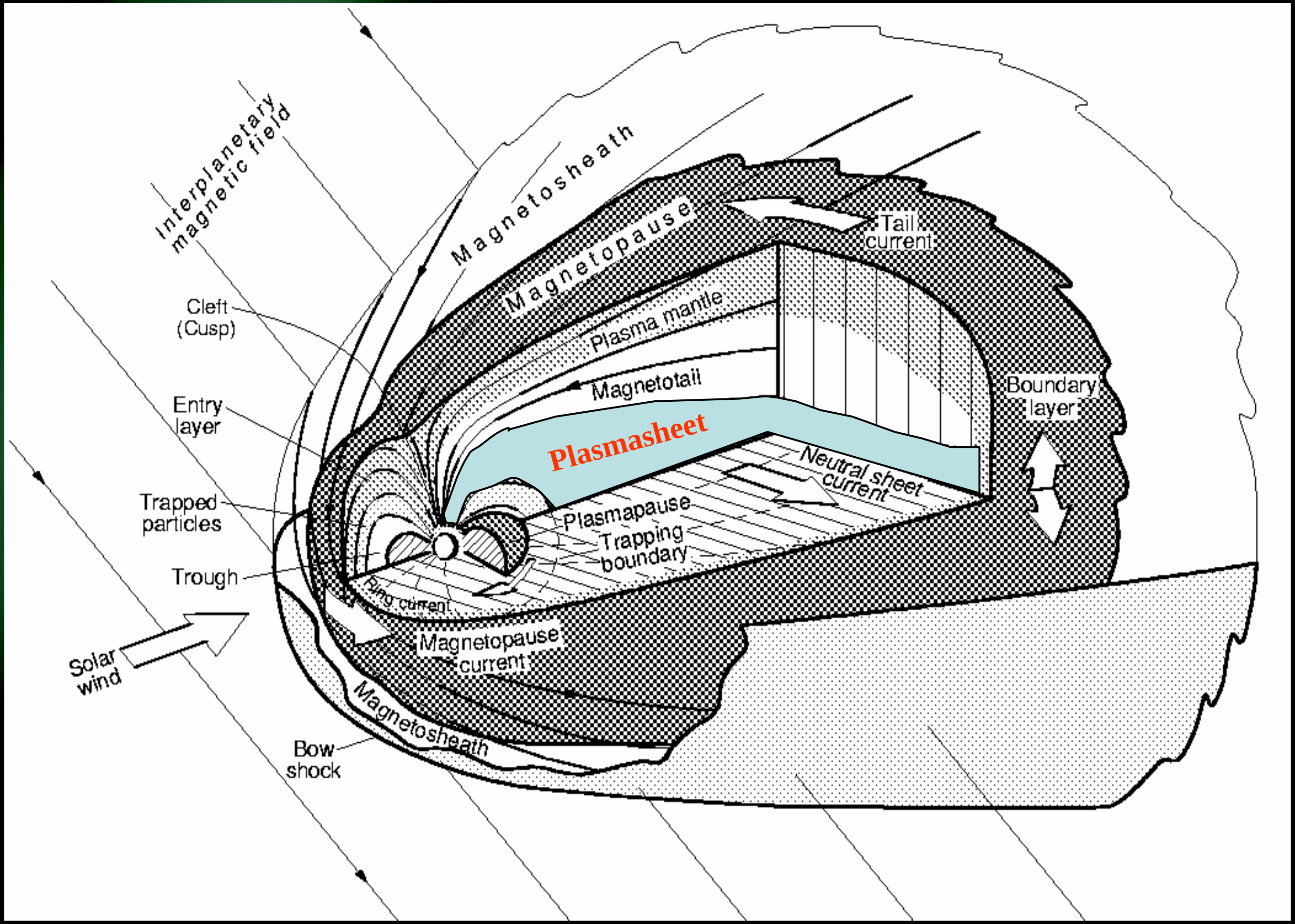

Auroral emissions

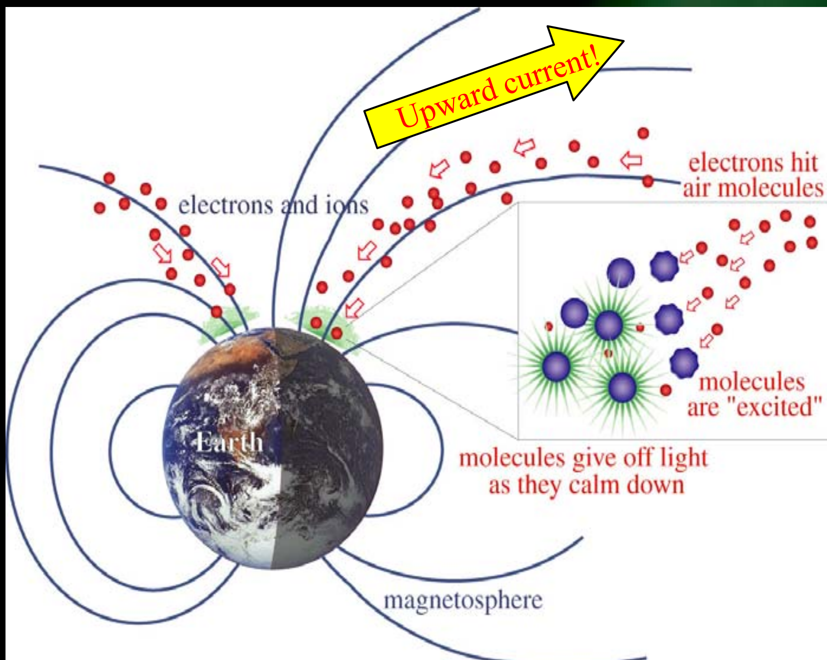

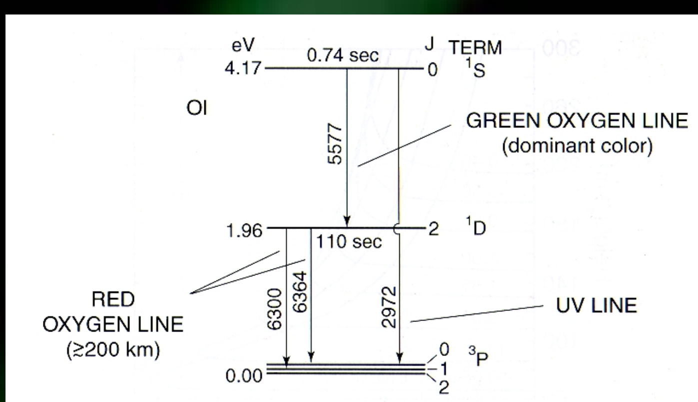

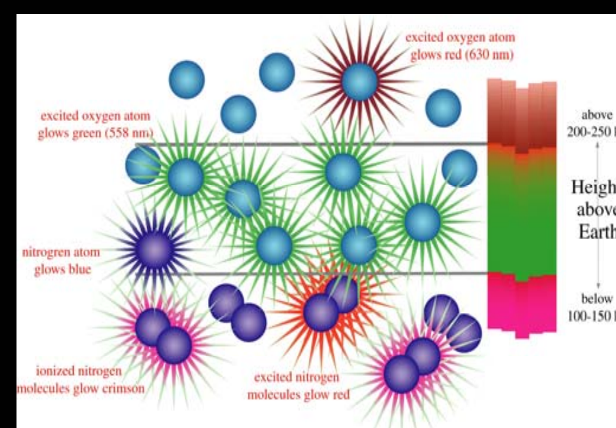

Homogenous auroral arcs

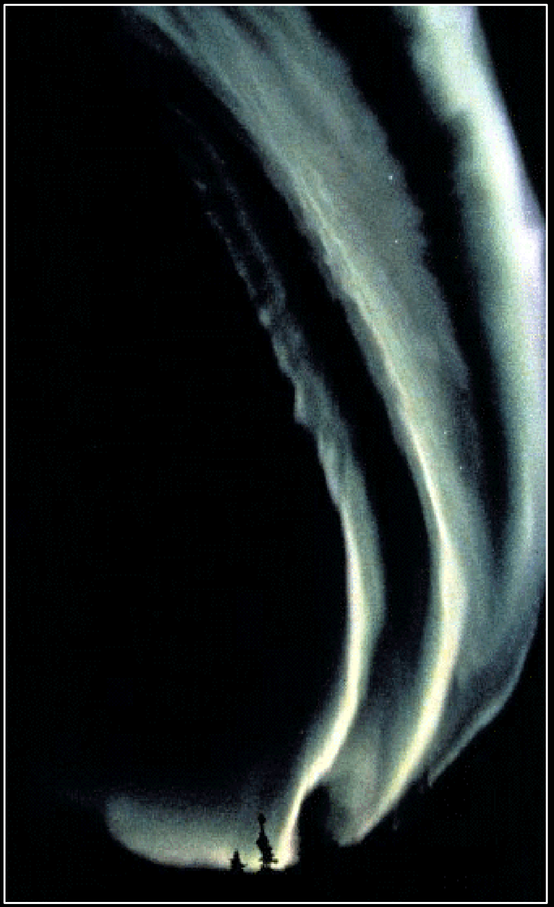

Particle motion in the geomagnetic field

gyration **longitudinal oscillation** **azimuthal drift**

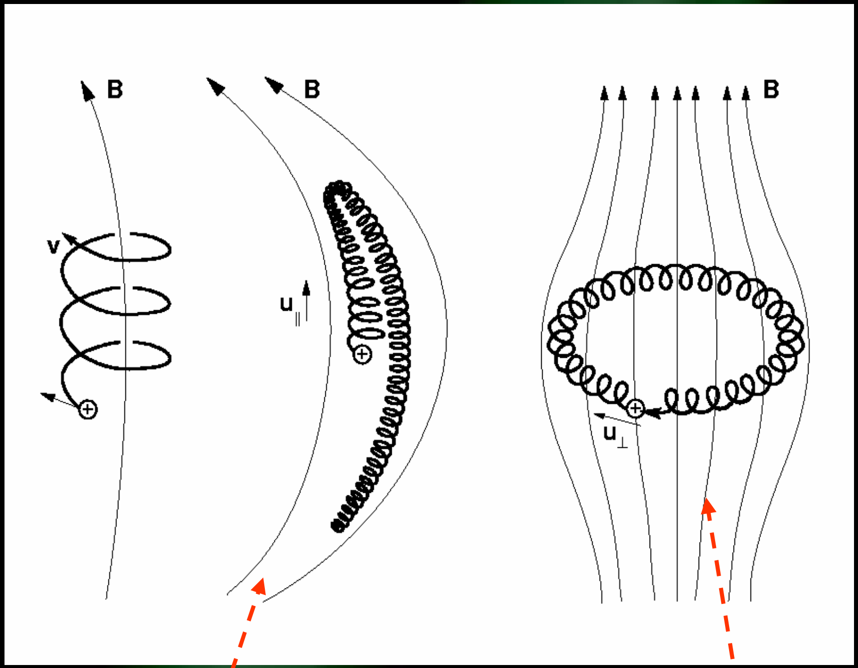

Magnetic mirror

grad B drift

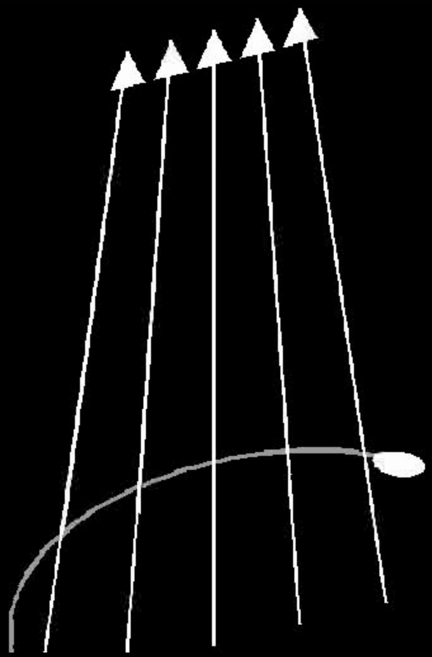

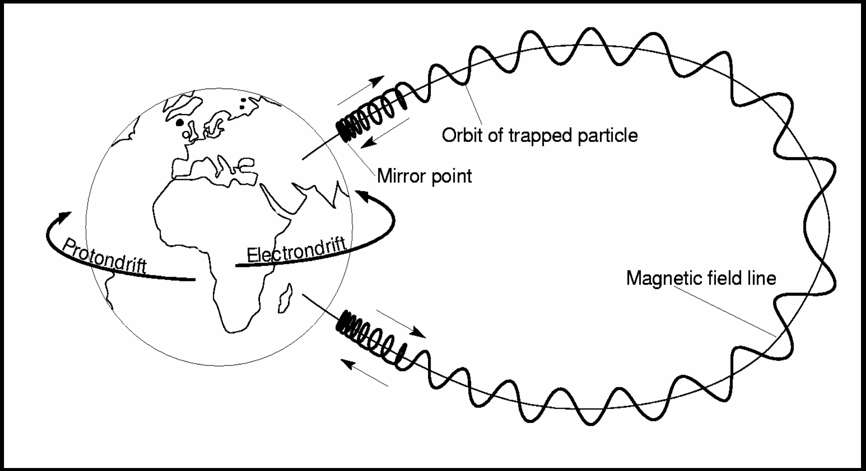

Magnetic mirror

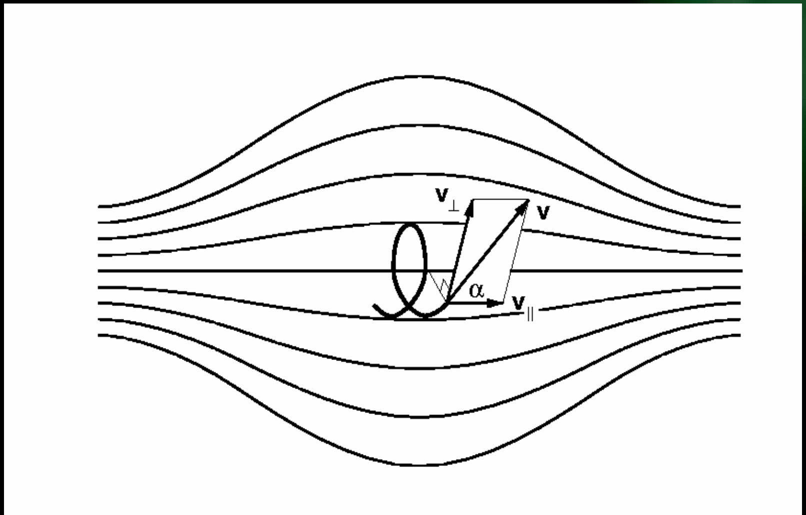

$mv^2/2$ constant

$$\frac{\sin^2\alpha}{B} = const$$

particle turns when $\alpha = 90°$

$$B_{turn} = B/\sin^2\alpha$$

If maximal B-field is B_{max} a particle with pitch angle α can only be turned around if

$$B_{turn} = B/\sin^2\alpha \le B_{max}$$

$$\alpha > \alpha_{lc} = \arcsin\sqrt{B/B_{max}}$$

The magnetic moment μ is an ***adiabatic invariant***.

$$\mu = \frac{mv_\perp^2}{2B} = \frac{mv^2\sin^2\alpha}{2B}$$

Particles in ***loss cone*** : $\alpha < \alpha_{lc}$

Magnetospheric convection

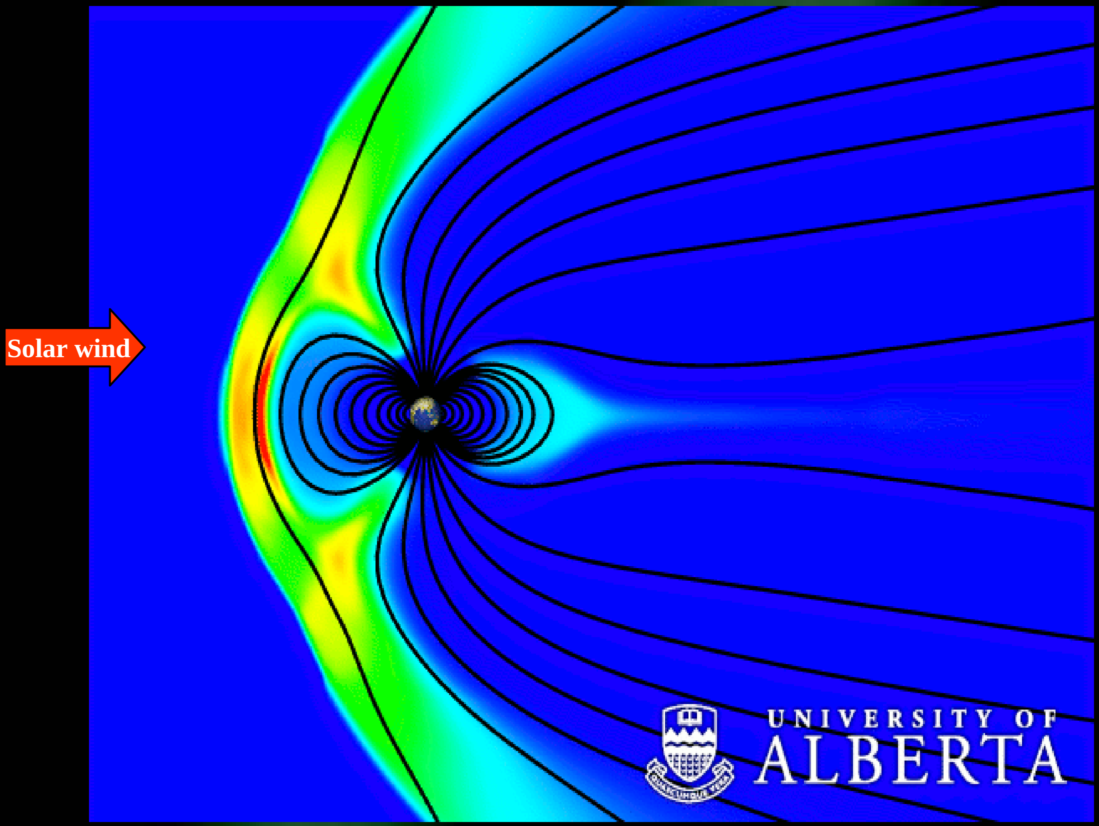

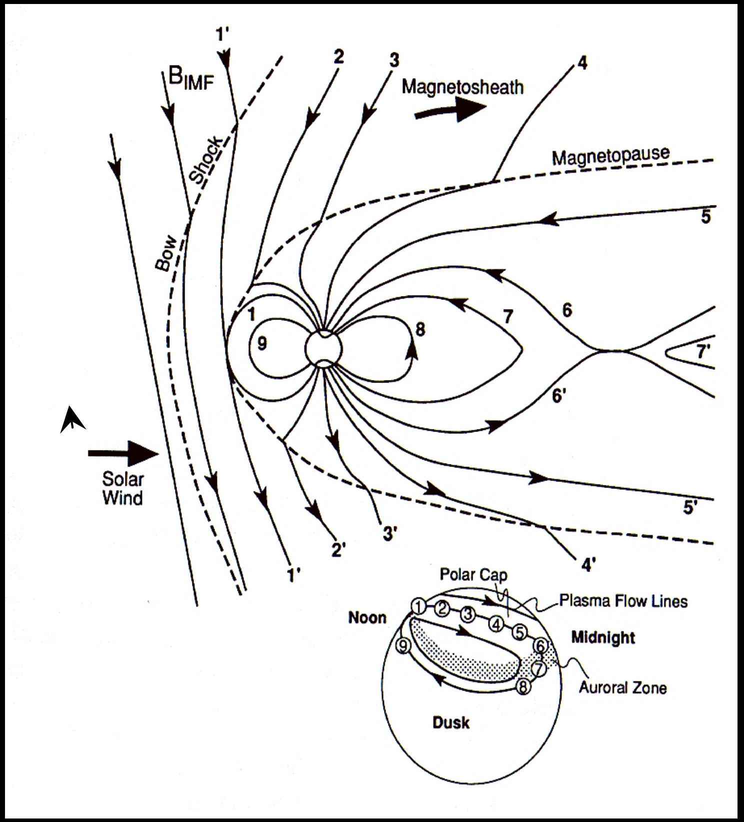

Atmospheric collisions - emissions

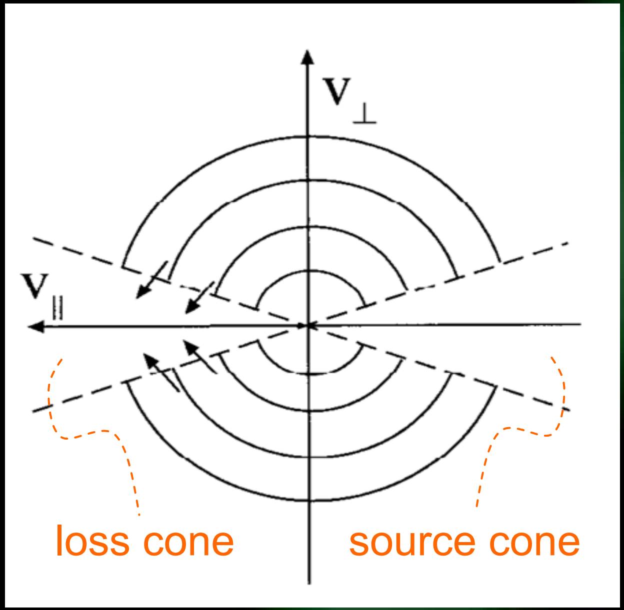

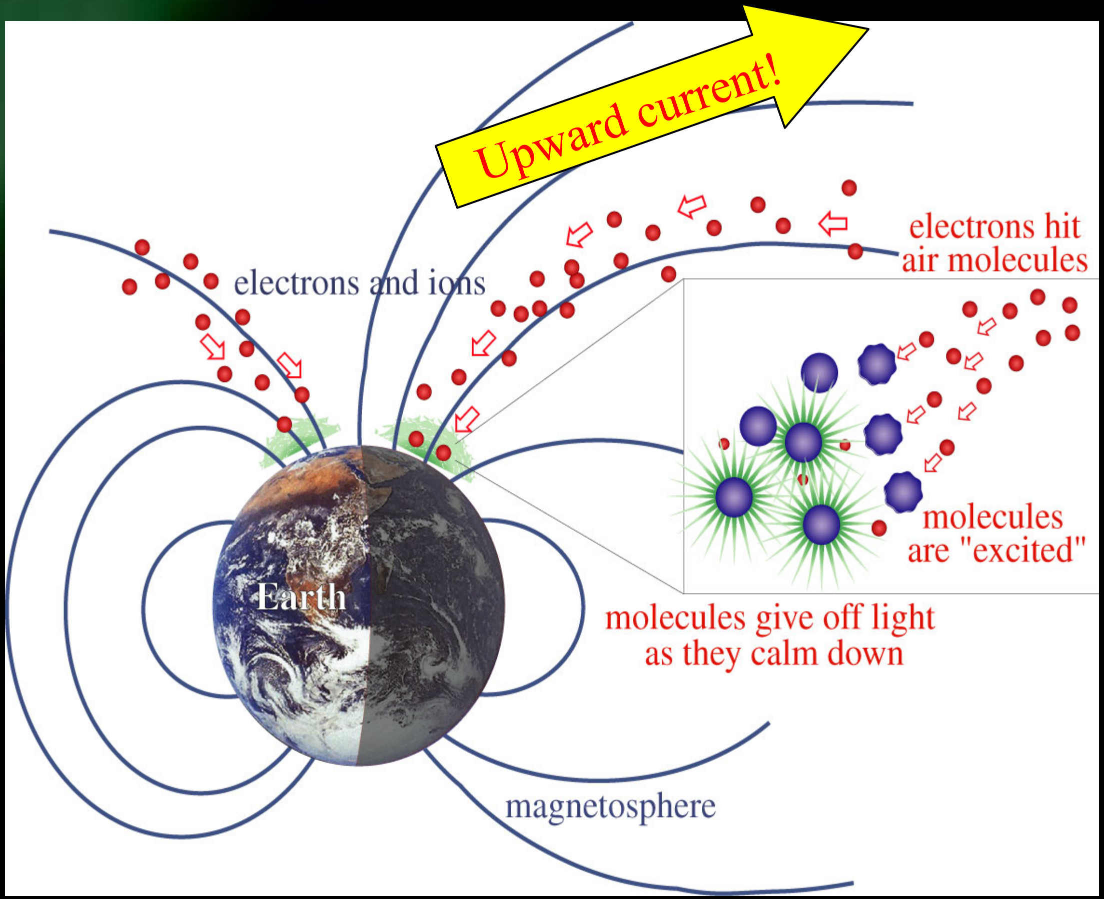

A typical auroral pass - CLUSTER

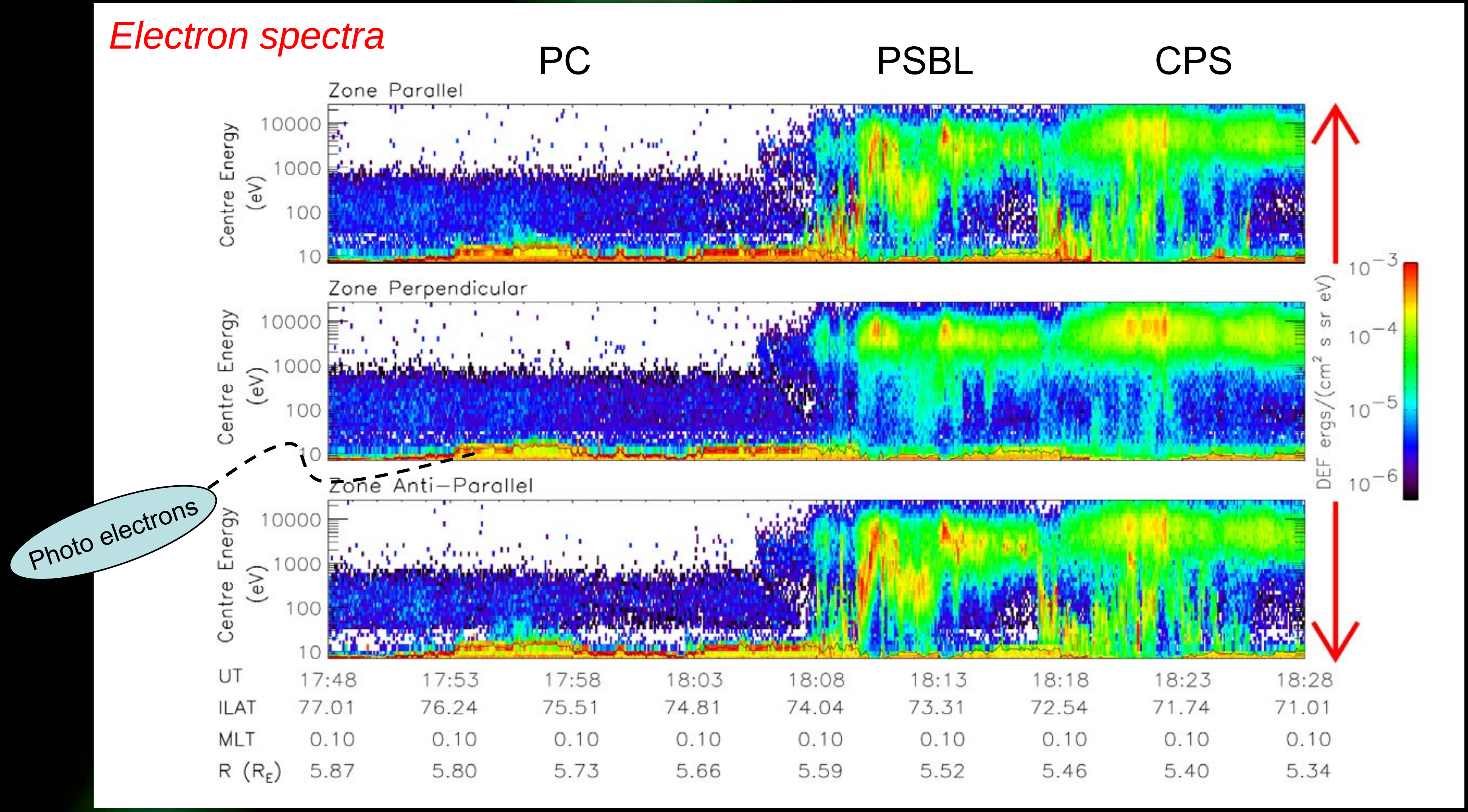

Auroral scales

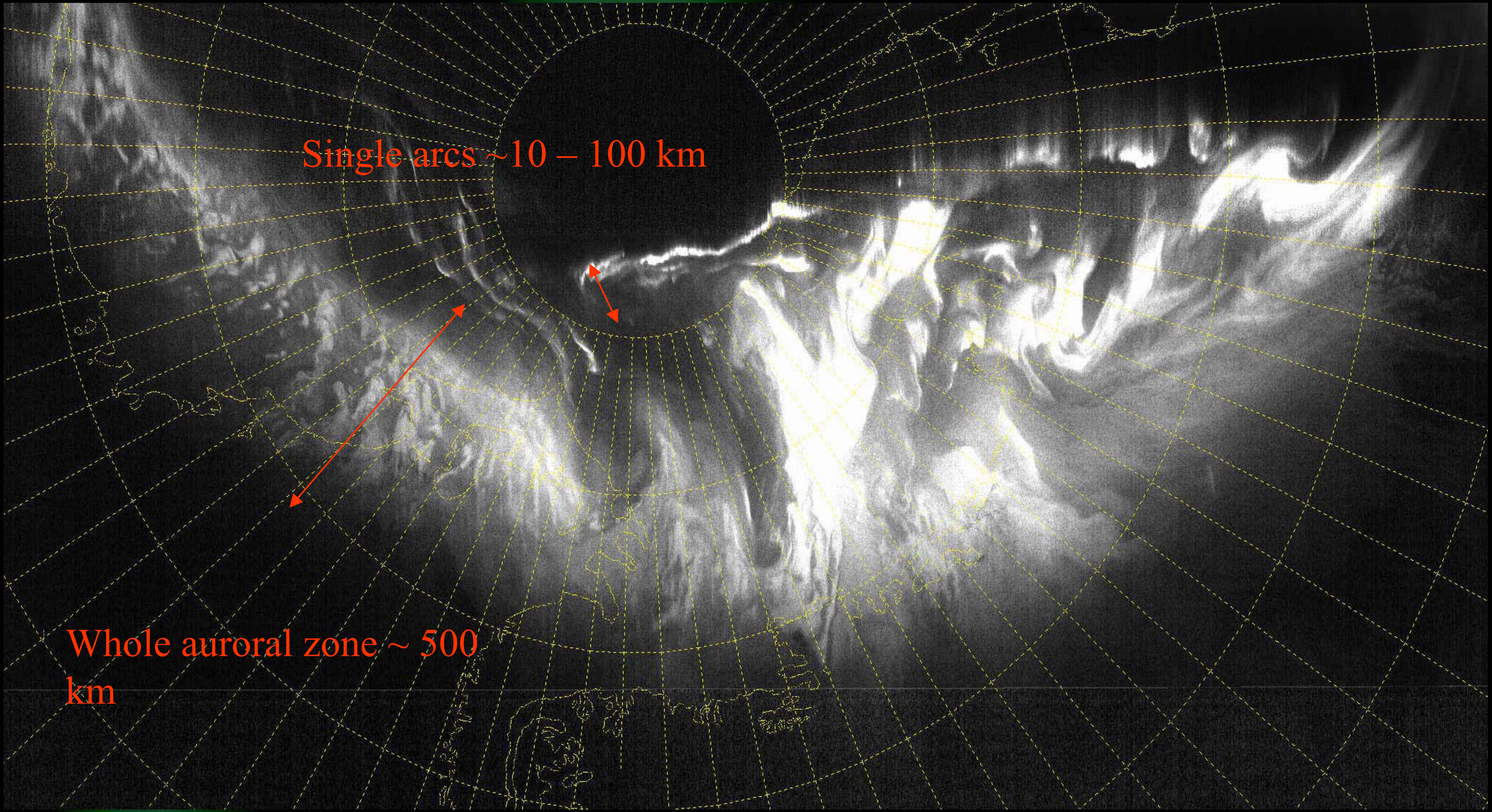

Photo from DMSP satellite

Birkeland currents in the auroral oval

Low geomagnetic activity High geomagnetic activity

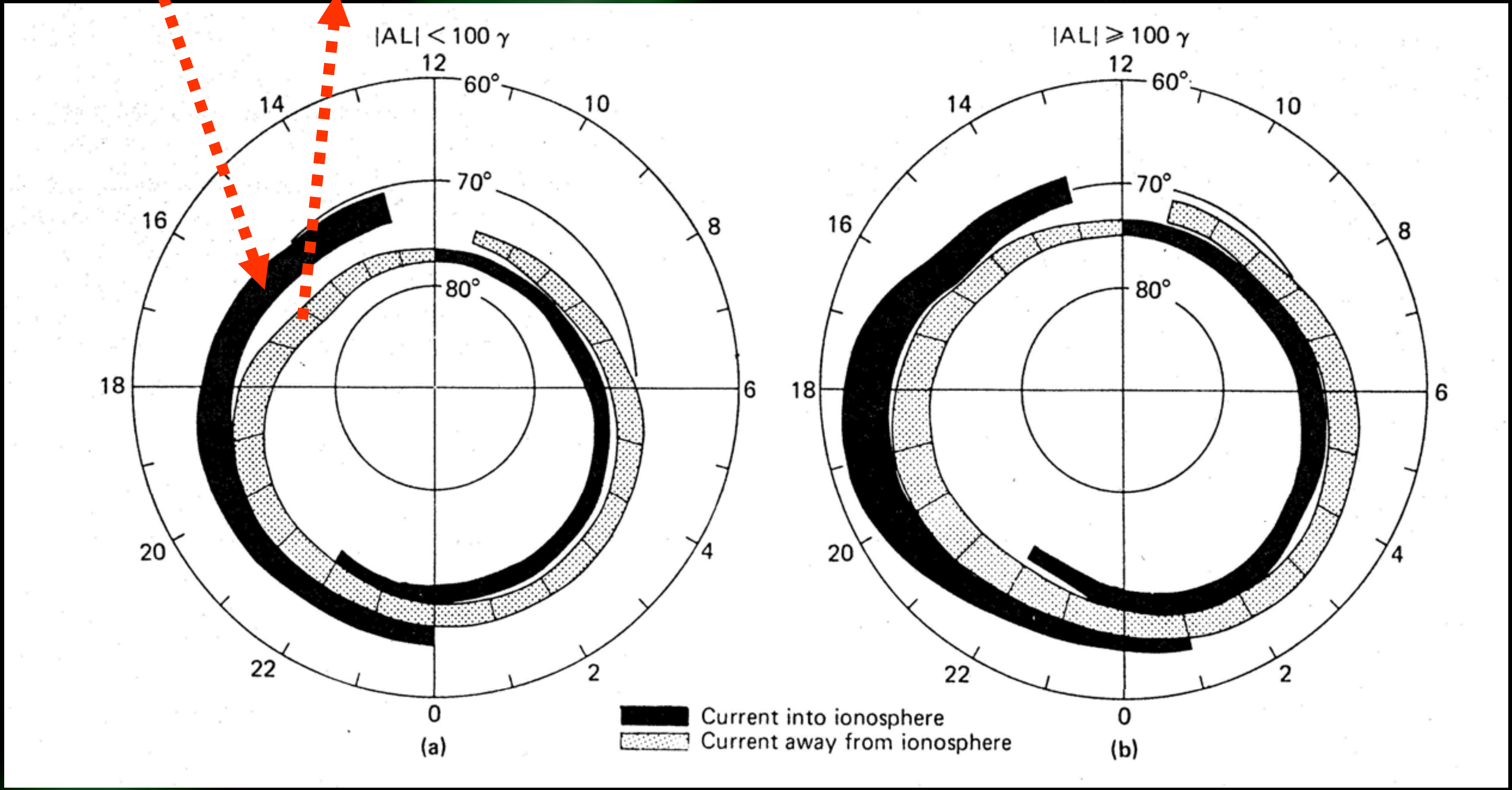

A typical auroral pass - FAST

ΔB_{EW}

dE-flux, e^-

PA, e^-

dE-flux, e^-

n-flux, e^-

E-flux, e^-

dE-flux, i^+

PA, i^+

E-perp (DC)

E (AC)

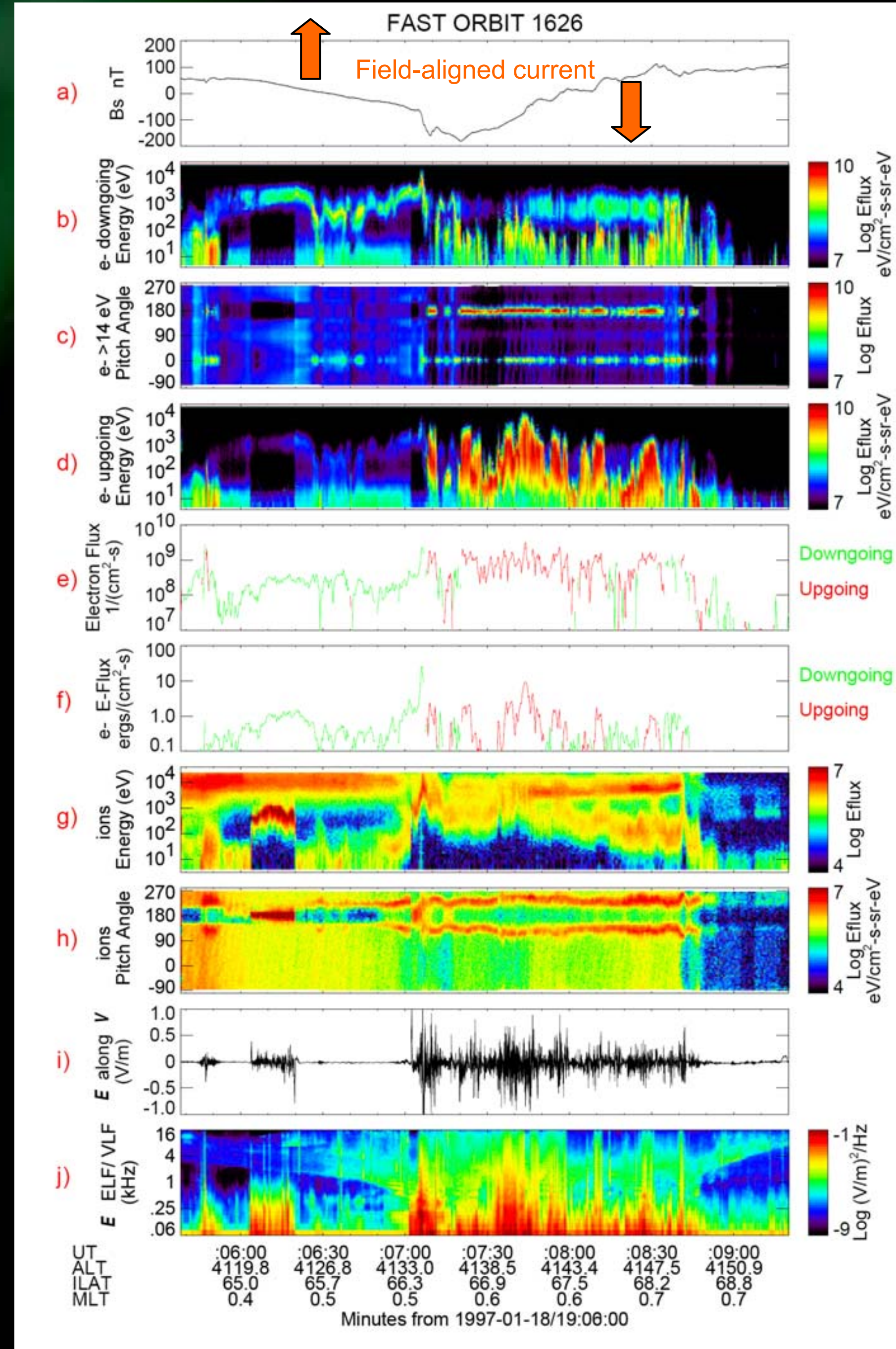

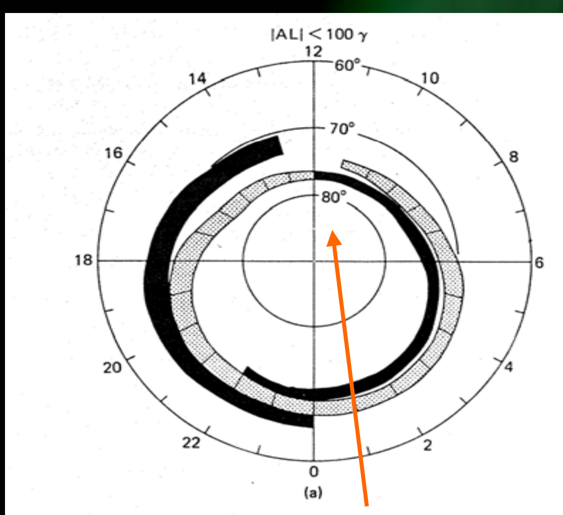

Current sheet approximation and Ampére's law

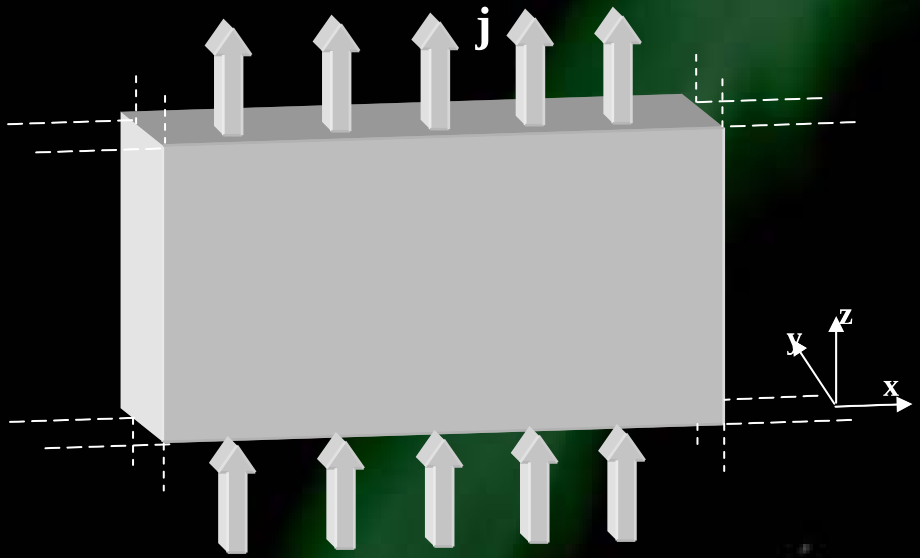

$$\left(\frac{\partial B_z}{\partial y}-\frac{\partial B_y}{\partial z},\ \frac{\partial B_x}{\partial z}-\frac{\partial B_z}{\partial x},\ \frac{\partial B_y}{\partial x}-\frac{\partial B_x}{\partial y}\right)=\mu_0\left(j_x,\ j_y,\ j_z\right)$$

But $\frac{\partial}{\partial x} = 0$ and $\frac{\partial}{\partial z} = 0$

$$\left(\frac{\partial B_z}{\partial y},\ 0,\ -\frac{\partial B_x}{\partial y}\right)=\mu_0\left(0,\ 0,\ j_z\right)$$

Ampére's law (no time dependence):

$$\nabla\times\mathbf{B}=\mu_0\mathbf{j}$$

$$\boxed{j_z=-\frac{1}{\mu_0}\frac{\partial B_x}{\partial y}}$$

Current sheet

Determination of current density by magnetic field measurement

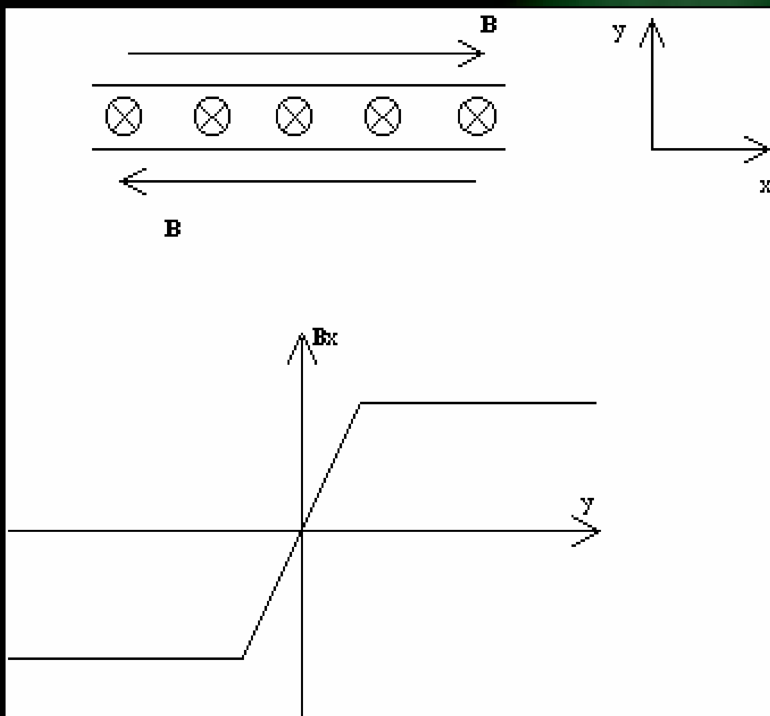

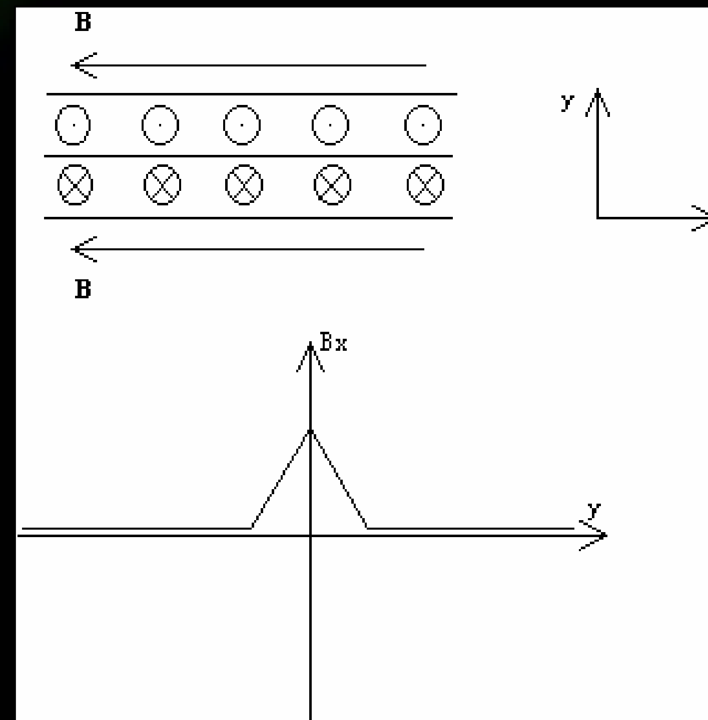

$$j_z = -\frac{1}{\mu_0}\frac{\partial B_x}{\partial y}$$

Upward and downward current regions

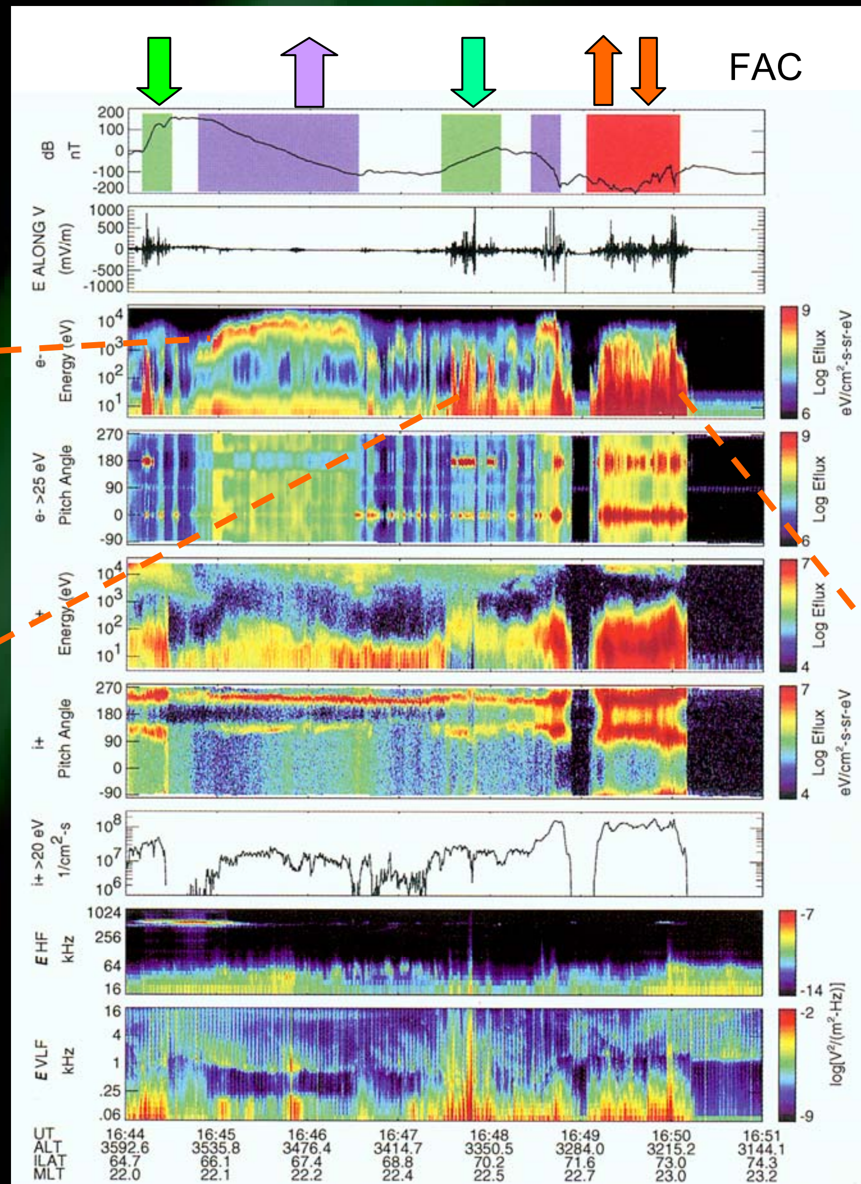

Inverted V

Upgoing electron beams

Alfvénic aurora

180° =

0° =

Upward current region

Inverted V arc

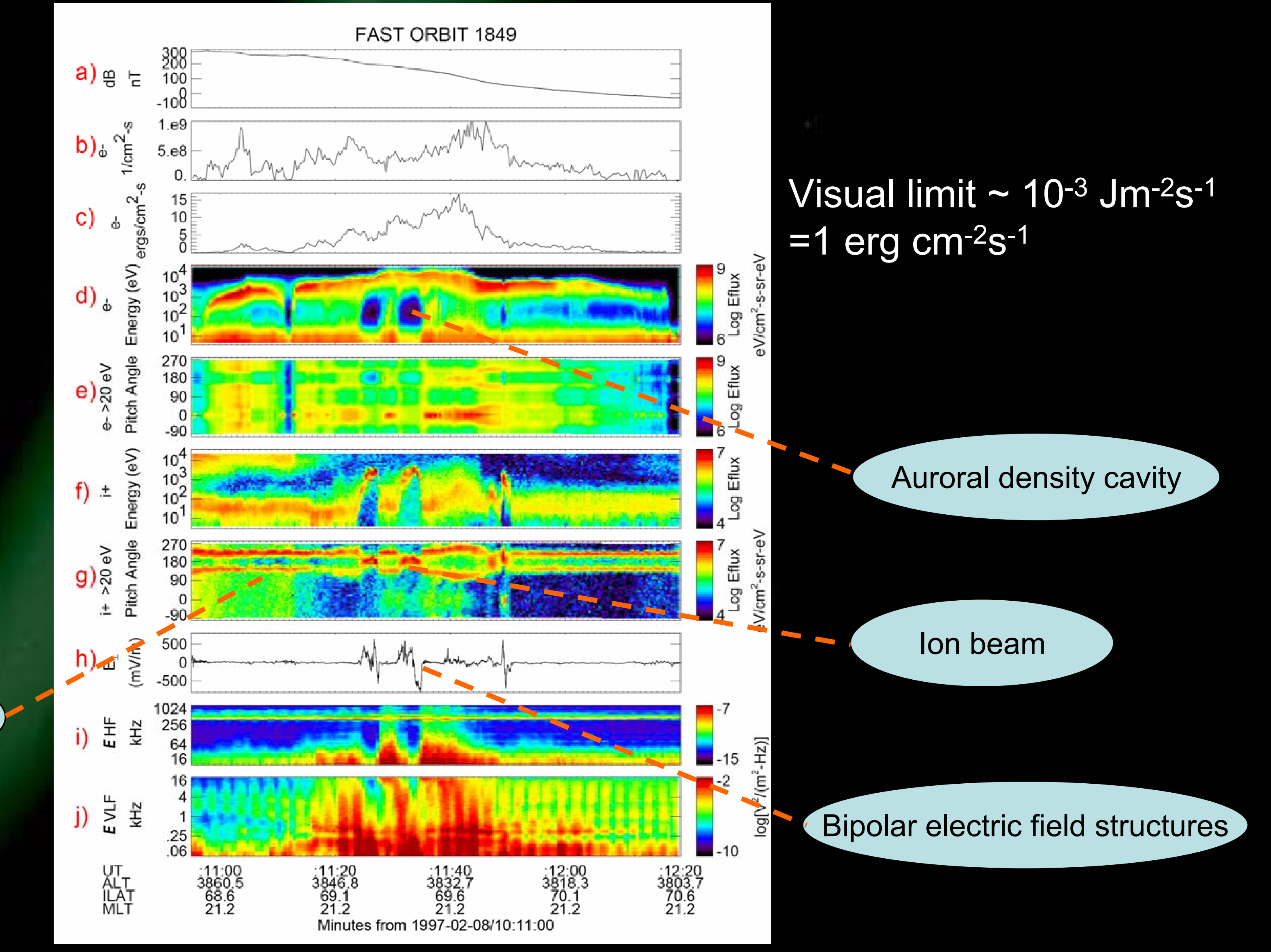

180° = ↑

0° = ↓

Visual limit ~ 10^{-3} $Jm^{-2}s^{-1}$ =1 erg $cm^{-2}s^{-1}$

Satellite signatures of U potential

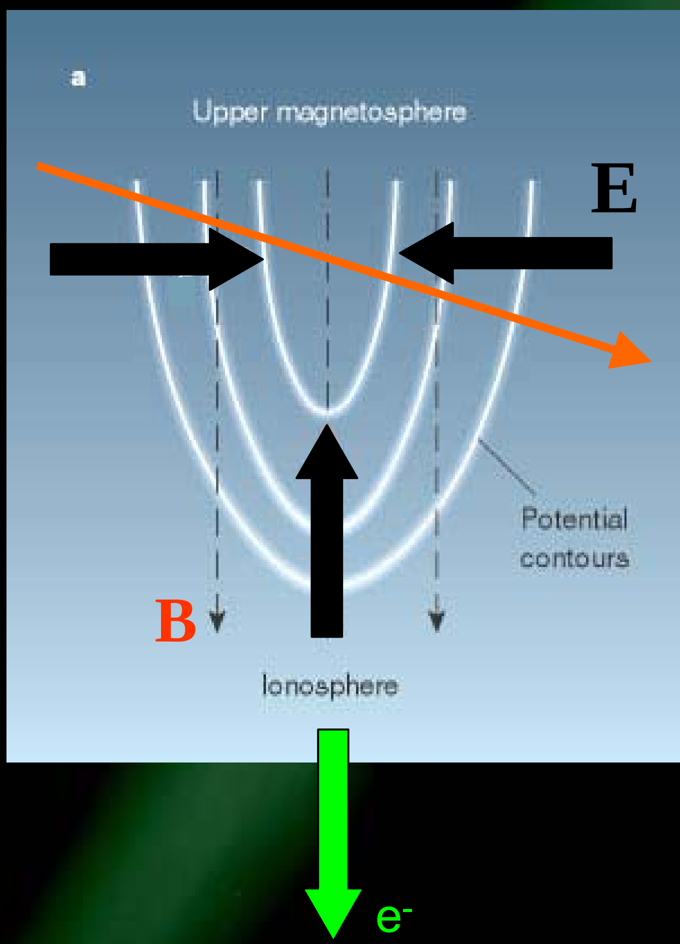

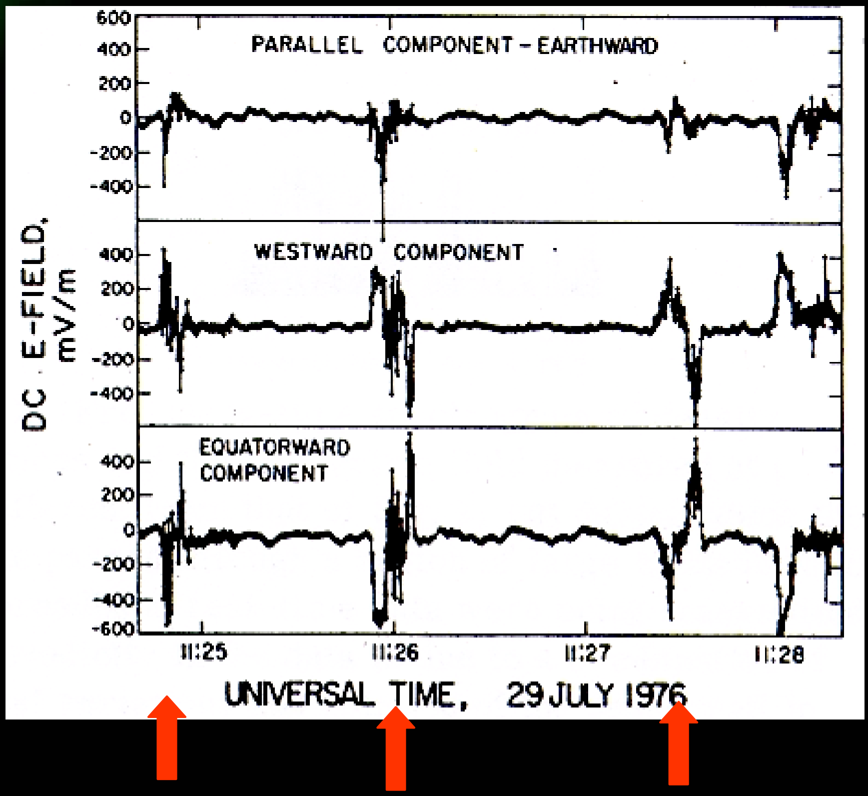

Measurements made by the ISEE satellite (Mozer et al., 1977)

Acceleration potential structure I

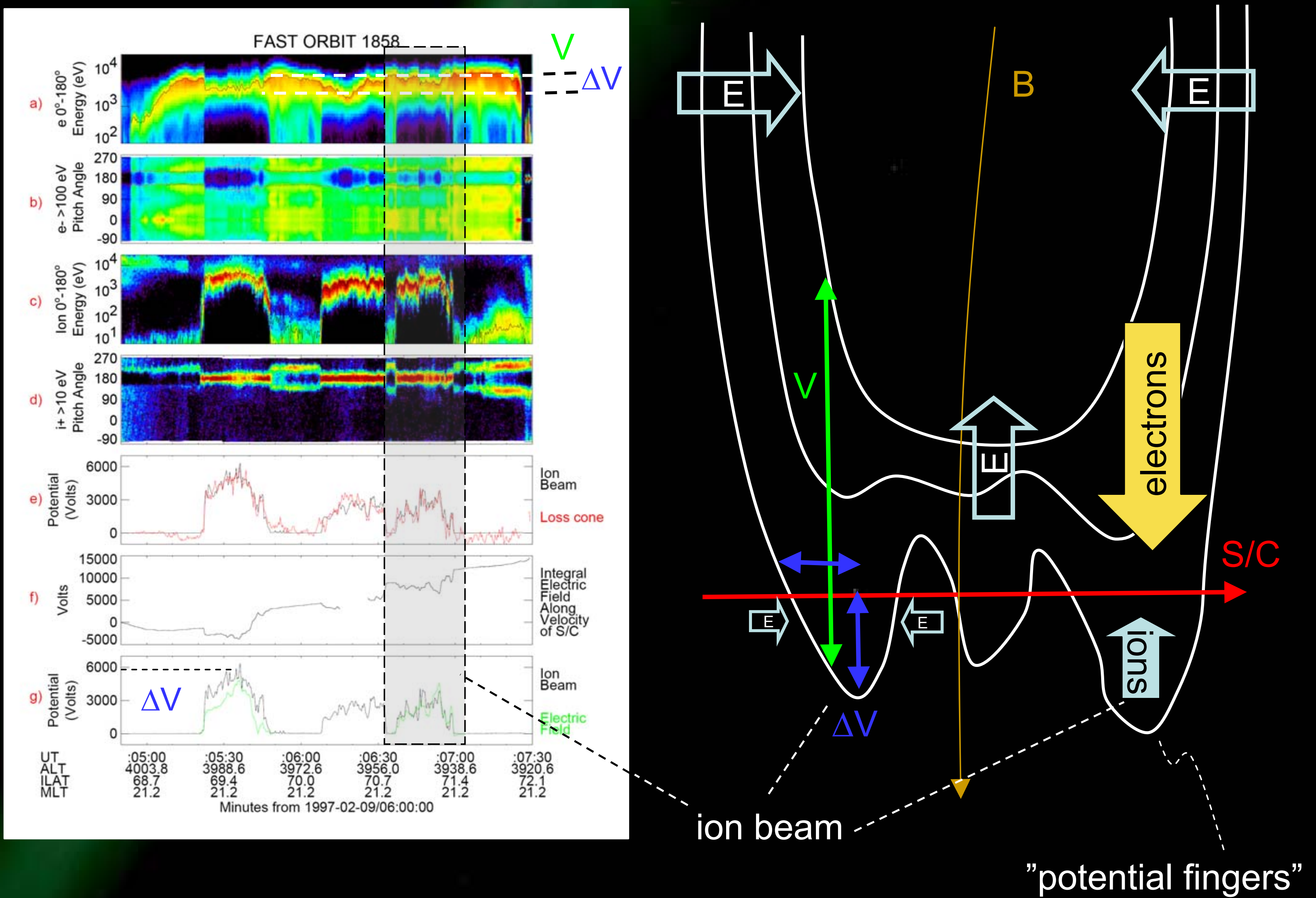

Acceleration potential structure II

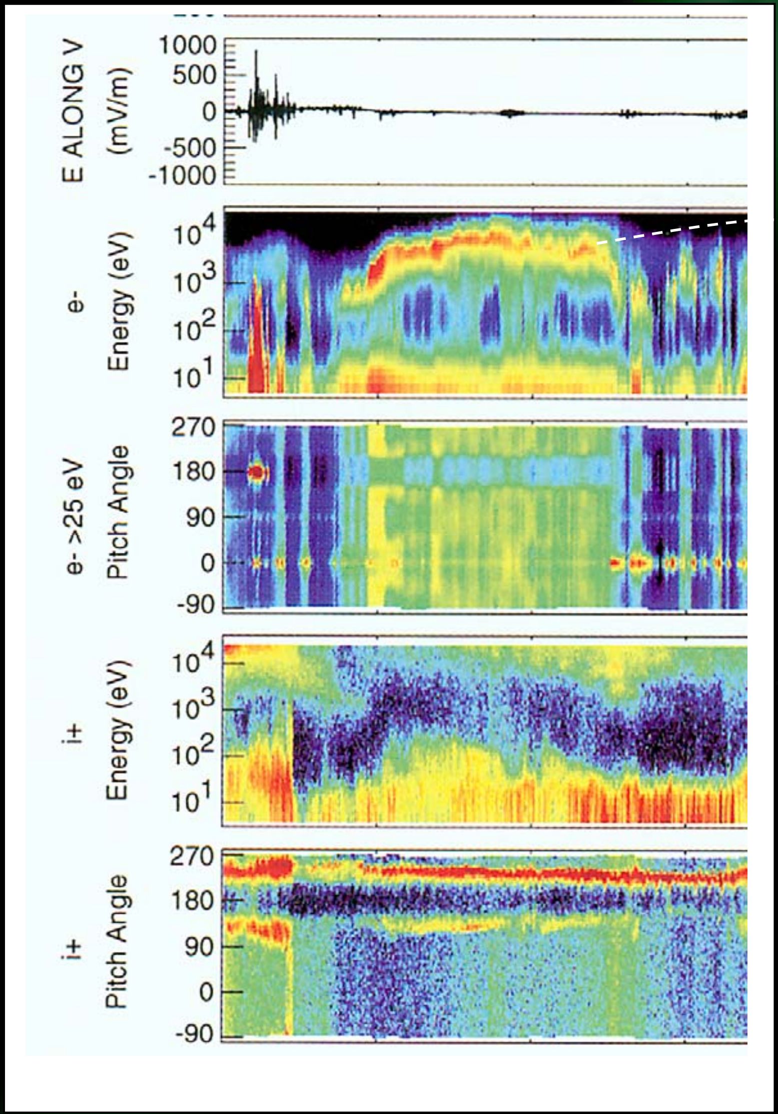

Localized regions of higher energy electrons without associated ion beams

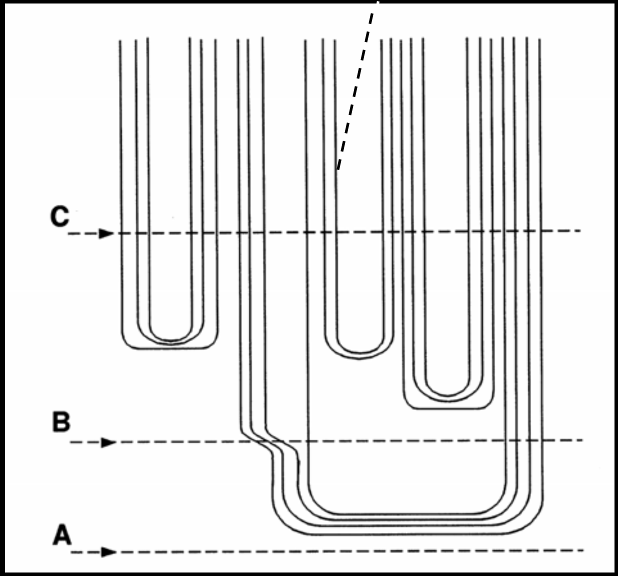

Why particle acceleration?

- The magnetosphere often acts as a current generator
- Electrons are accelerated downwards by upward E-field.
- This increases the pitch-angle of the electrons, and more electrons can reach the ionosphere, where the current can be closed.

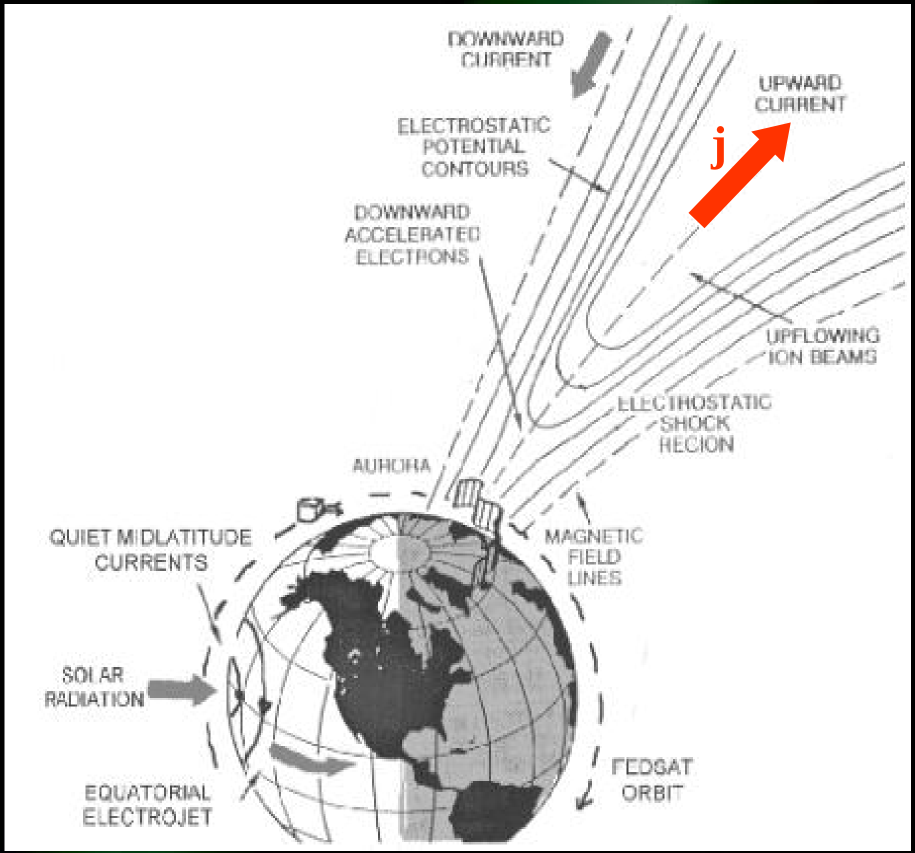

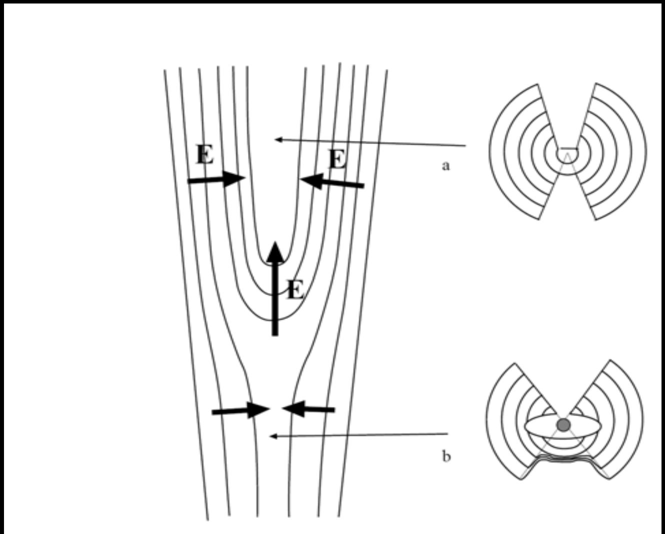

Auroral currents – Knight relation

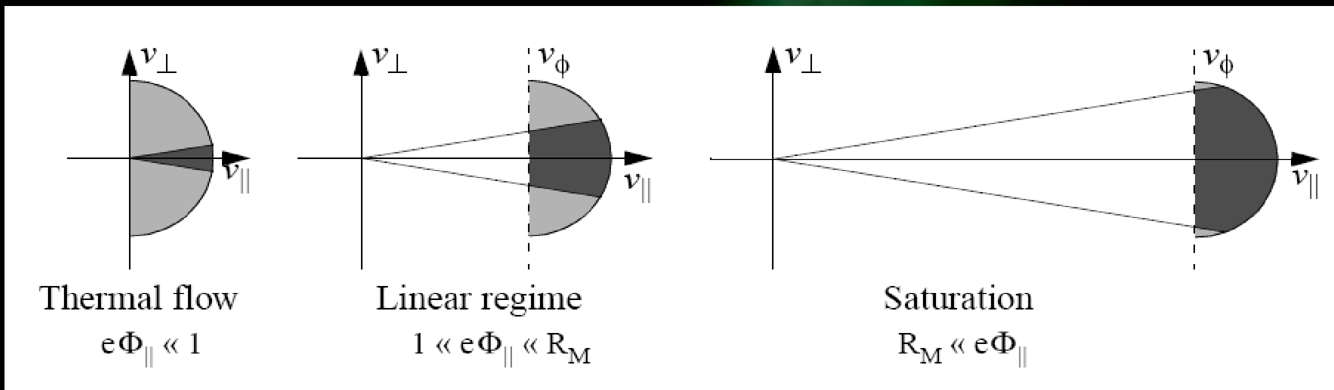

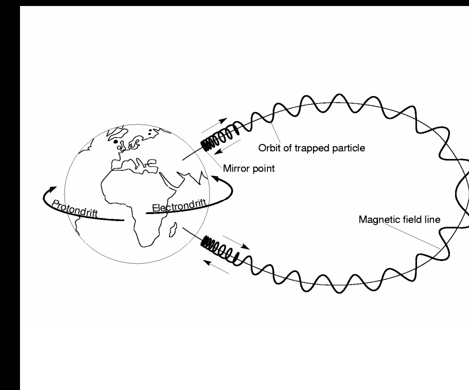

Fraction of particles in the loss cone:

$$f = \frac{\pi\theta_{lc}}{2\pi} \sim \frac{B_{ms}}{B_{ion}} \sim 2\times10^{-4}$$

Thermal current:

$$j_{\parallel,ms} = n_0 e v_{th} f$$

$$j_{\parallel,ion} = n_0 e v_{th} f \frac{B_{ms}}{B_{ion}} =$$

$$= n_0 e v_{th} \frac{B_{ms}}{B_{ion}} \frac{B_{ion}}{B_{ms}} = n_0 e v_{th} \approx$$

$$\left[n_e = 0.1\,\mathrm{cm}^{-3}, T_e = 1\,\mathrm{keV} \right] \approx$$

$$\sim 1\,\mu\mathrm{A/m}^2$$

Apply a parallel potential drop:

$$j_{\parallel,ion} = n_0 e v_{th} \frac{B_{ion}}{B_{ms}} \left[1 - \frac{e^{-xe\Phi_\parallel / T_e}}{1+x} \right]$$

Linear regime :

$$j_{//,ion} \approx n_0 e v_{th} \frac{e\Phi_{//}}{k_B T_e} = K\Phi_{//}$$

$$K = \frac{e^2 n_0}{\sqrt{2\pi m_e k_B T_e}} \sim 10^{-9}\ \mathrm{S/m}^2$$

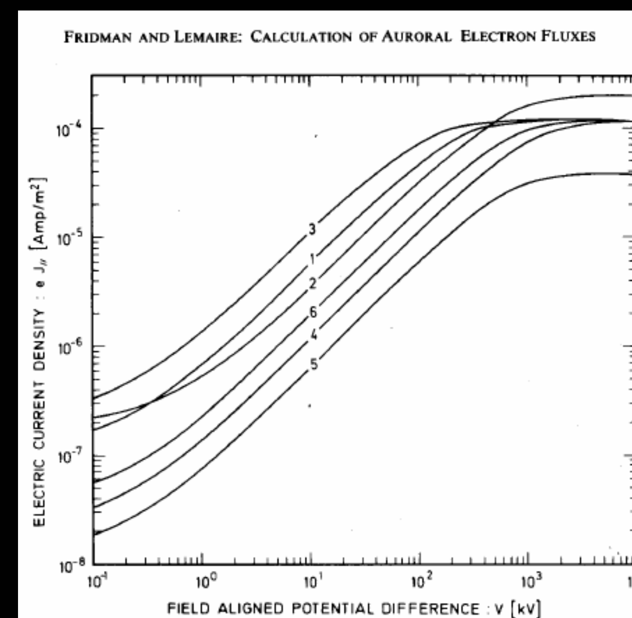

$$v_{th} = \sqrt{T_e / 2\pi m_e} \qquad x = \frac{1}{B_I / B_0 - 1}$$

Particle distributions associated with inverted V's

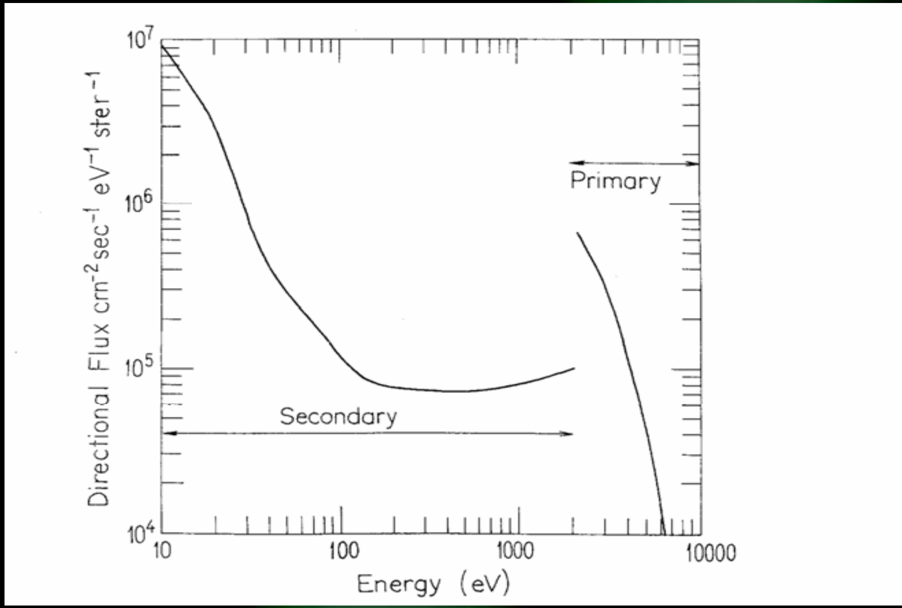

Model of cold beam producing secondaries (Evans, 1974)

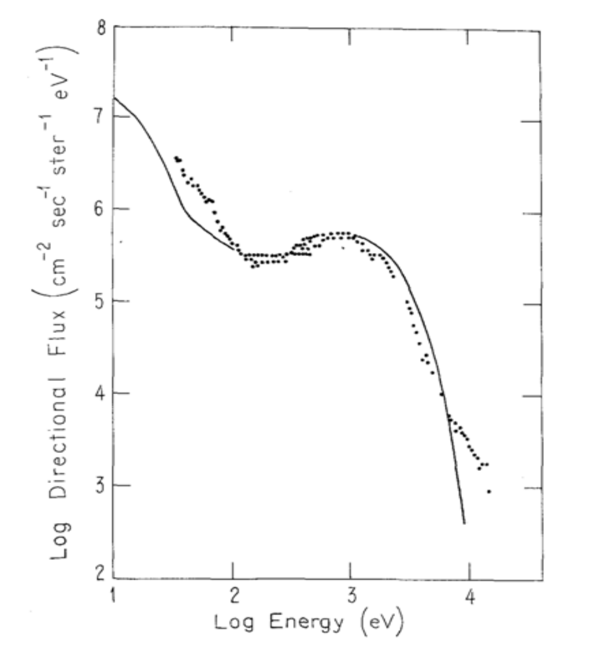

Model of hot electron beam and second<aries (Evans, 1974). Data from Franck and Ackerson, 1971

Auroral cavity and trapped populations

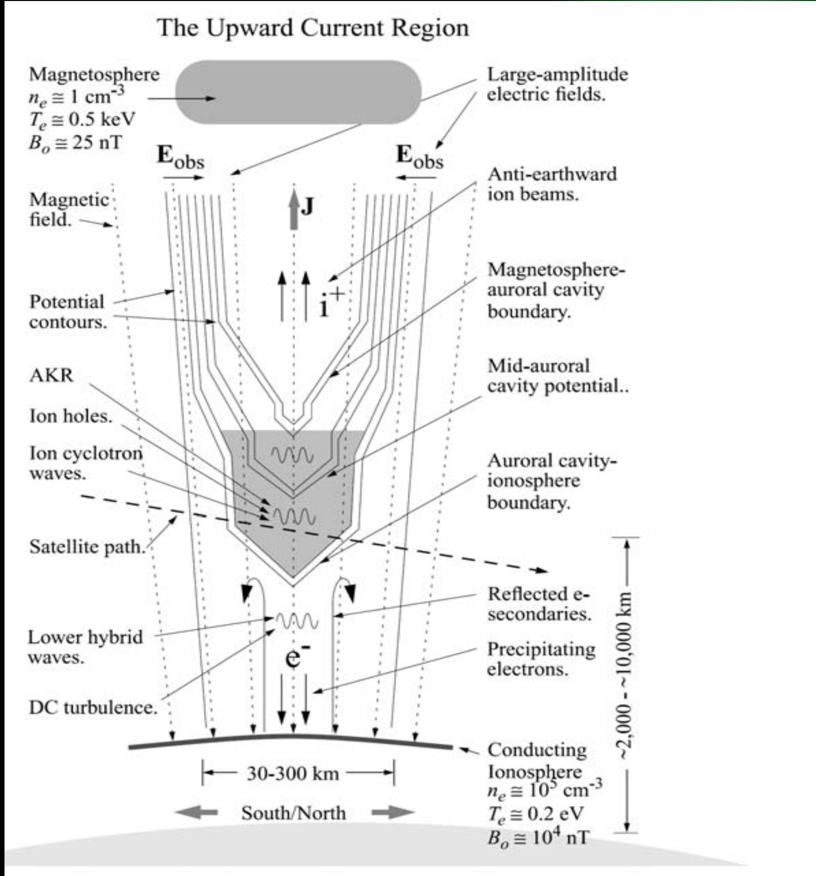

ed cartoon of the upward current region of the aurora. The potential conto
ltitude and high-altitude acceleration region with the auroral cavity in b

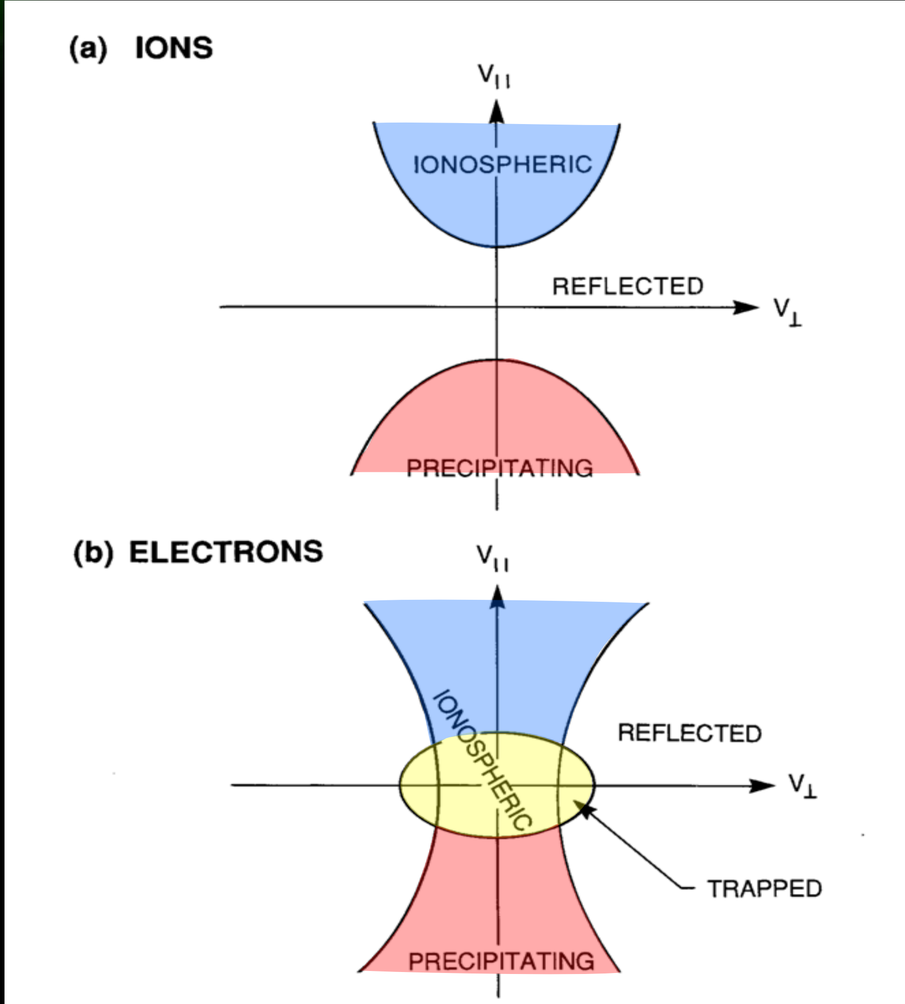

Accelerated Maxwellian

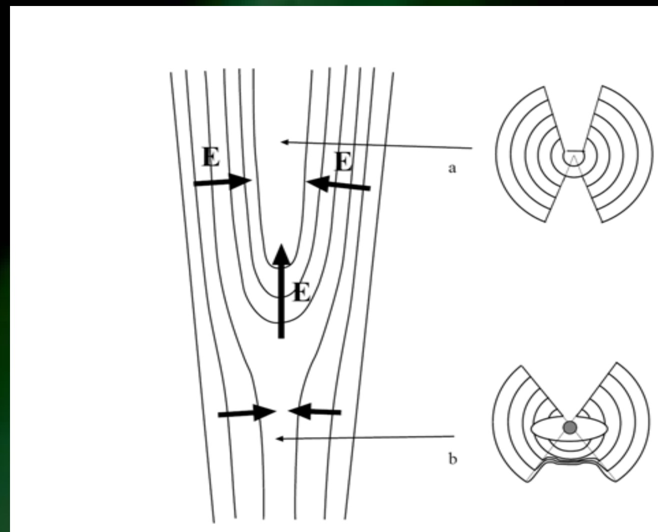

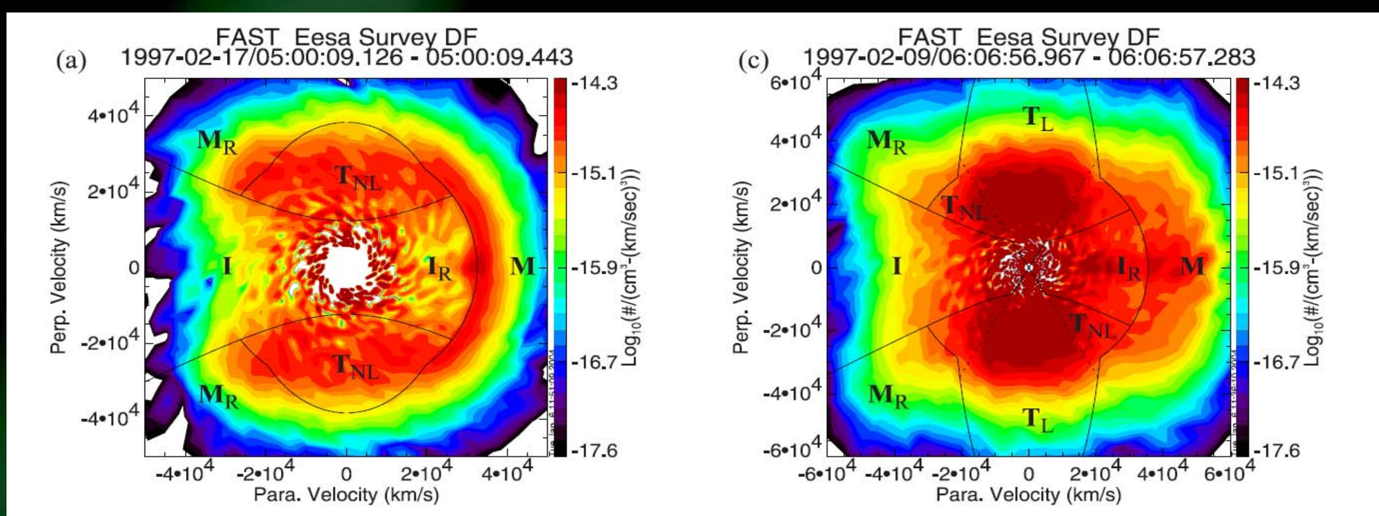

Acceleration regions

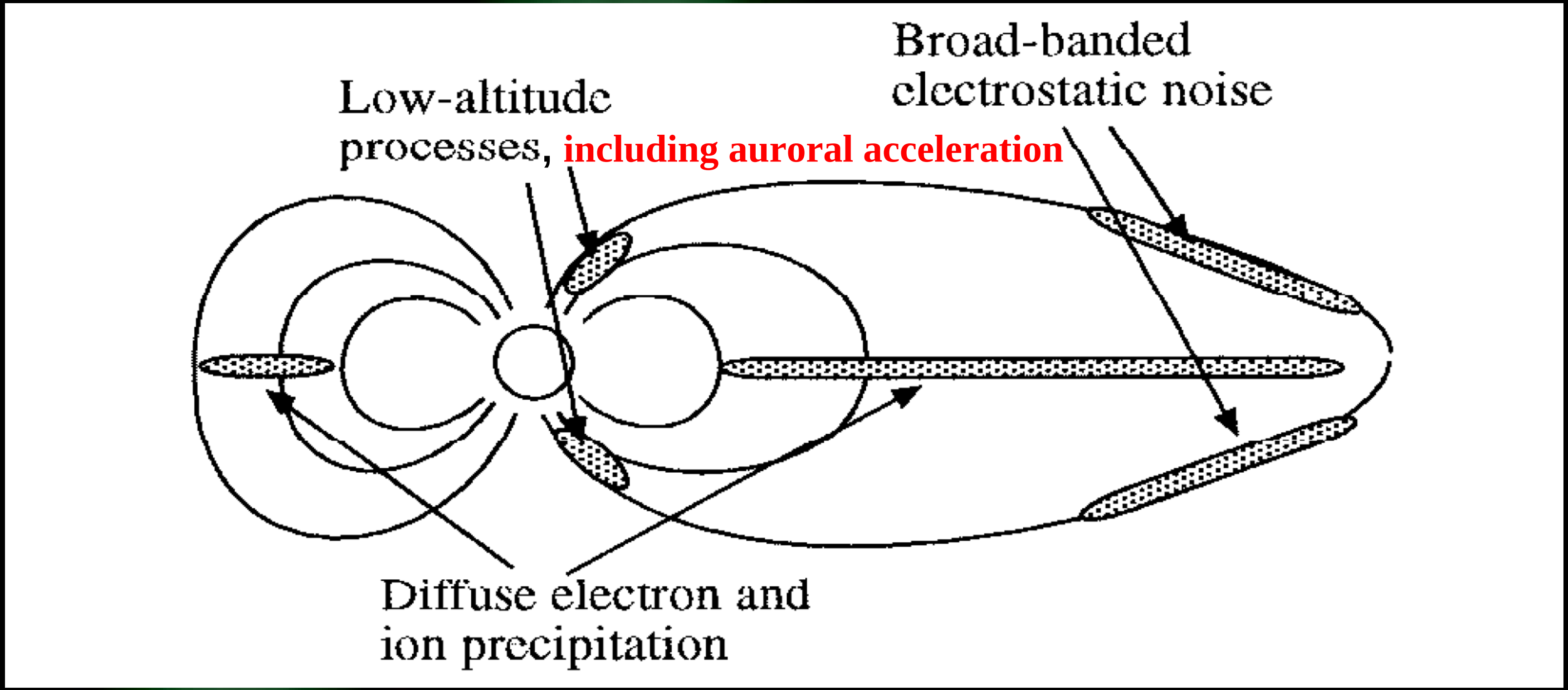

Koskinen

Auroral acceleration region typically situated at altitude of 1-3 R_E

Mapping of auroral electric fields

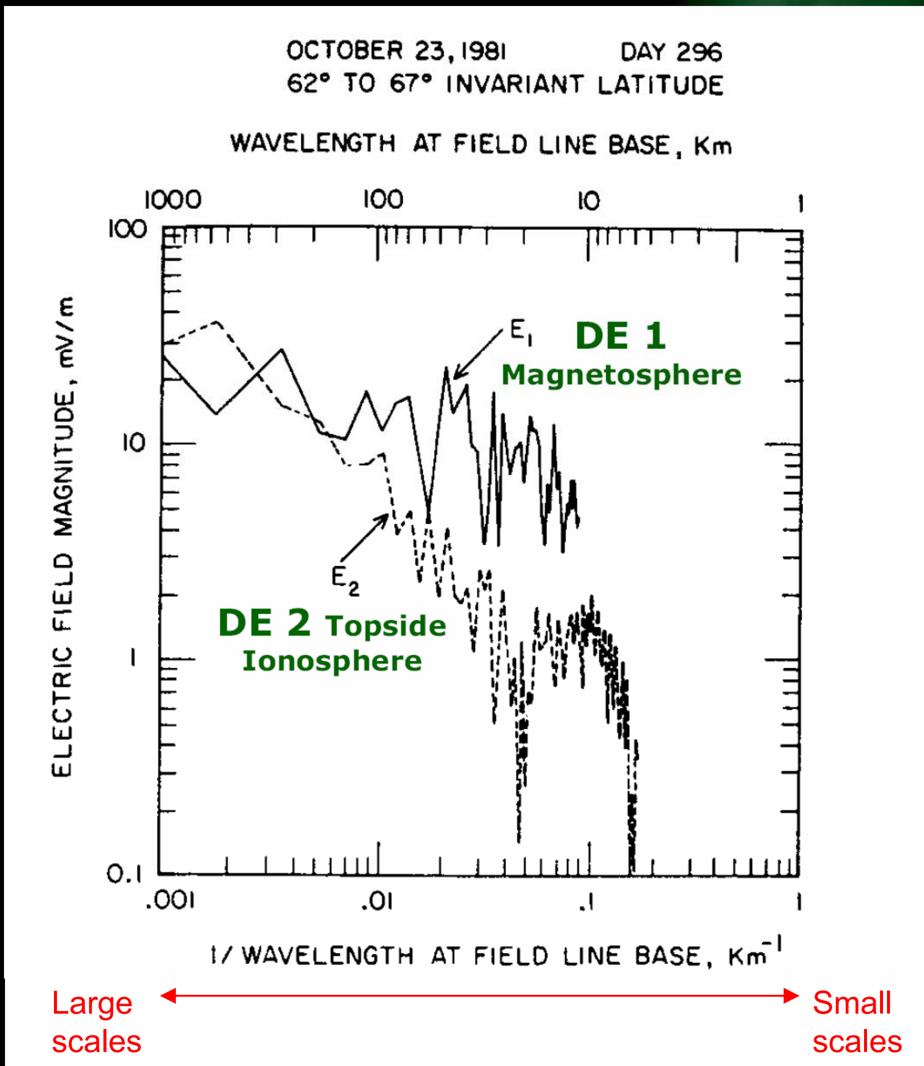

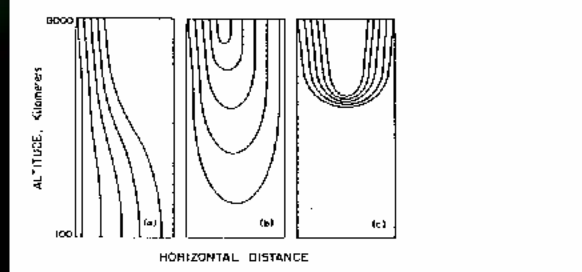

Figura 8. Contururi echipotentiale posibile in zona de accelerare (v. text). Din Hudson and Mozer (1978)

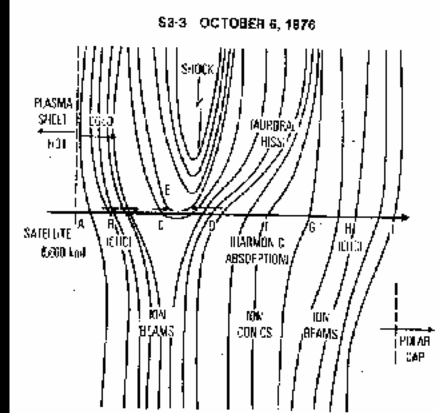

Figura 9. Reconstructia calitativa a contururilor echipotentiale din date S3-3. Figura ilustreaza 1 minut de observatii. Din Mizera et al. (1982)

Experimental results, comparison between Dynamics Explorer 1 and 2 at different altitudes. (*Weimer et al., 1985*)

Static, medium-scale MI-coupling

MI-coupling critical scale size II

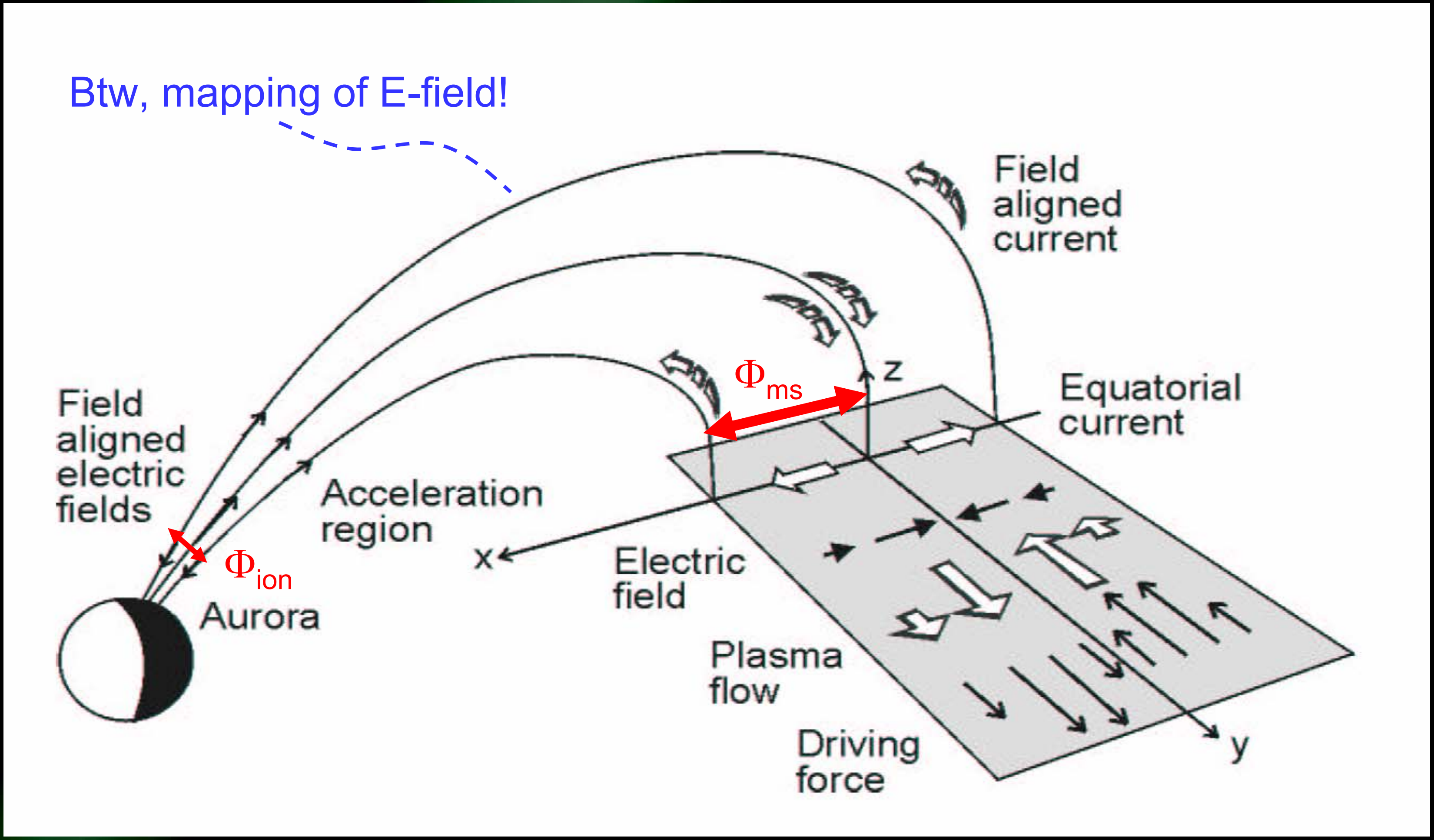

Static, medium-scale MI-coupling

MI-coupling critical scale size III

$$j_{//} = \Sigma_P \nabla_\perp \cdot \mathbf{E}_\perp + \mathbf{E}_\perp \cdot \nabla_\perp \Sigma_P + (\mathbf{E}_\perp \times \nabla_\perp \Sigma_H) \cdot \hat{\mathbf{b}}$$

$$j_{//} = \Sigma_P \nabla_\perp \cdot \mathbf{E}_\perp$$

$$j_{||} = K \Delta \Phi_{//} = K(\Phi_{ms} - \Phi_{ion})$$

$$K(\Phi_{ms} - \Phi_{ion}) = \Sigma_P \nabla_\perp \cdot \mathbf{E}_{\perp ion}$$

$$K(\Phi_{ms} - \Phi_{ion}) = \Sigma_P \nabla_\perp^2 \Phi_{ion}$$

$$K(\Phi_{ms} - \Phi_{ion}) \approx \Sigma_P \frac{\Phi_{ion}}{L^2}$$

$$\Phi_{ion} = \left(1 + \frac{\Sigma_P}{KL^2}\right)^{-1} \Phi_{ms}$$

When L >> $\sqrt{\frac{\Sigma_P}{K}}$: $\Phi_{ion} \approx \Phi_{ms}$

When L << $\sqrt{\frac{\Sigma_P}{K}}$: $\Phi_{ion} \ll \Phi_{ms}$

The last case means $|\Phi_{ms}| \approx |\Delta\Phi_{//}|$

Static, medium-scale MI-coupling

MI-coupling critical scale size

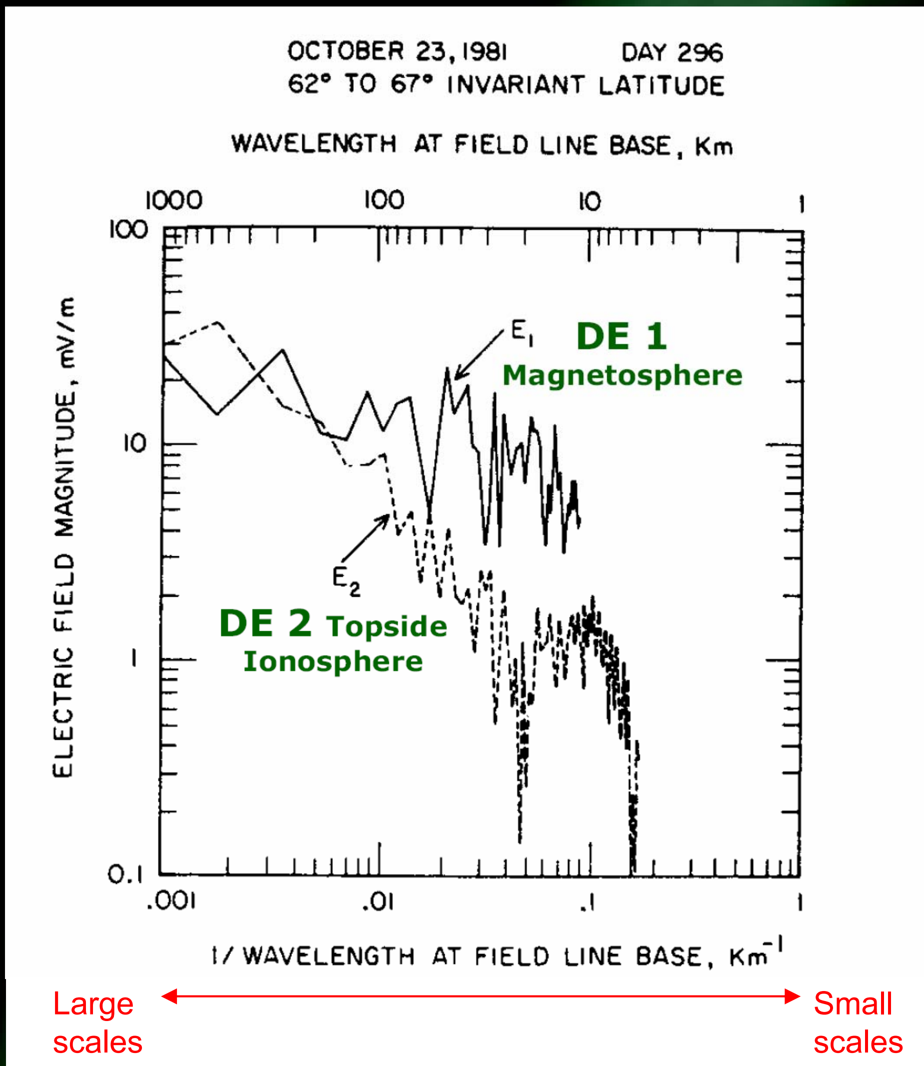

Experimental results, comparison between Dynamics Explorer 1 and 2 at different altitudes. (*Weimer et al., 1985*)

1/ WAVELENGTH AT FIELD LINE BASE, Km^{-1}

Fig. 4. Electric field spectrums from day 296 (October 23) of 1981. The spectrums are obtained from a Fourier transform of the electric field data between 62° and 67° invariant latitude. The solid line shows the spectrum of the electric field measured by DE 1. The solid line shows the spectrum of the electric field measured by DE 2. The ordinate values are obtained from the square root of the "spectral power density." The actual units are mV m^{-1} $km^{1/2}$.

Weimer et al, 1985